Computational and Structural Biotechnology Journal 19 (2021) 3394–3406

COMPUTATIONAL AND STRUCTURAL BIOTECHNOLOGY JOURNAL

journal homepage: www.elsevier.com/locate/csbj

Structural basis of the selective activation of enzyme isoforms: Allosteric response to activators of β1- and β2-containing AMPK complexes

Elnaz Aledavood [1], Alessia Forte, Carolina Estarellas [*,3], F. Javier Luque [*,2]

Department of Nutrition, Food Science and Gastronomy, Faculty of Pharmacy and Food Sciences, Institute of Biomedicine (IBUB) and Institute of Theoretical and Computational Chemistry (IQTCUB), University of Barcelona, Av. Prat de la Riba 171, Santa Coloma de Gramenet 08921, Spain

ARTICLE INFO

Article history:
Received 3 March 2021
Received in revised form 30 May 2021
Accepted 30 May 2021
Available online 05 June 2021

Keywords:
Enzyme isoforms
Allostery
Enzyme activation
AMPK
Structure-function relationships
Protein dynamics

ABSTRACT

AMP-activated protein kinase (AMPK) is a key energy sensor regulating the cell metabolism in response to energy supply and demand. The evolutionary adaptation of AMPK to different tissues is accomplished through the expression of distinct isoforms that can form up to 12 complexes, which exhibit notable differences in the sensitivity to allosteric activators. To shed light into the molecular determinants of the allosteric regulation of this energy sensor, we have examined the structural and dynamical properties of β1- and β2-containing AMPK complexes formed with small molecule activators A-769662 and SC4, and dissected the mechanical response leading to active-like enzyme conformations through the analysis of interaction networks between structural domains. The results reveal the mechanical sensitivity of the α2β1 complex, in contrast with a larger resilience of the α2β2 species, especially regarding modulation by A-769662. Furthermore, binding of activators to α2β1 consistently promotes the pre-organization of the ATP-binding site, favoring the adoption of activated states of the enzyme. These findings are discussed in light of the changes in the residue content of β-subunit isoforms, particularly regarding the β1Asn111 → β2Asp111 substitution as a key factor in modulating the mechanical sensitivity of β1- and β2-containing AMPK complexes. Our studies pave the way for the design of activators tailored for improving the therapeutic treatment of tissue-specific metabolic disorders.

1. Introduction

Protein isoforms provide complexity to the structural and functional space of the human proteome [1]. Diverse mechanisms, such as genetic changes in protein-coding regions, alternative splicing and post-translational alterations, mediate the formation of isoforms, enriching the functional diversity by modulating enzymatic activities, molecular interactions and subcellular localizations [2,3] In this context, disclosing the molecular basis of the structural variation between isoforms is critical for understanding their functional adaptation to different tissues and organs, and for the design of therapeutic approaches tailored to the spatio-temporal context of diseases [4–7].

The evolutionary adaptation of protein isoforms is a key aspect of mammalian adenosine monophosphate-activated protein kinase (AMPK), which can form up to 12 different combinations according to the tissue-dependent expression of isoforms identified for the three structural components required for full activity [8–10]. This can be understood from the role played as a fuel-sensing enzyme in preserving the cellular energy homeostasis [11,12], since AMPK activation reduces the rate of anabolic pathways and up-regulates catabolic processes, resulting in increased levels of ATP. Furthermore, AMPK is implicated in metabolic disorders such as obesity and type 2 diabetes, cardiovascular diseases and cancer [13–15], attracting widespread interest as a therapeutic target [16].

AMPK is a heterotrimeric complex consisting of a catalytic α-subunit and two regulatory (β and γ) components, which are encoded by multiple genes, including two α (α1, α2), two β (β1, β2), and three γ (γ1, γ2, γ3) isoforms [17,18]. The catalytic subunit has a Ser/Thr kinase domain at the N-terminus and its C-terminus is necessary for the formation of the complex with the other components. The β-subunit has a central carbohydrate-binding module (CBM) that mediates AMPK interaction with glycogen, and the C-terminal region acts as a scaffold for the heterotrimeric assembly.

* Corresponding authors.
E-mail addresses: cestarellas@ub.edu (C. Estarellas), fjluque@ub.edu (F. Javier Luque).
[1] ORCID: 0000-0002-4837-7849.
[2] ORCID: 0000-0002-8049-3567.
[3] ORCID: 0000-0002-0944-9053.

https://doi.org/10.1016/j.csbj.2021.05.056

The γ-subunit has four tandem repeats of the cystathionine β-synthase (CBS) domain and contains four adenine nucleotide binding sites, which mediate the allosteric activation of the kinase activity by AMP, enabling AMPK to react to subtle fluctuations in the AMP/ATP ratio [19,20].

Due to its role in energy homeostasis, AMPK is finely regulated by different mechanisms [10], such as phosphorylation of α2Thr172 in the activation loop of the kinase domain. Thus, binding of AMP to the γ-subunit, in conjunction with Thr172 phosphorylation by upstream kinases such as LKB1 and CaMKKβ, converts the inactive enzyme into an active species, which is several thousand-fold more active [20,21]. AMPK can also be indirectly activated by compounds such as metformin, phenformin and oligomycin [22], which increase the intracellular levels of AMP. Finally, a direct activation of AMPK can be triggered by modulators such as the thienopyridone drug A-769662 (Table 1) [23], which binds to the so-called allosteric drug and metabolite (ADaM) site located at the interface between α- and β-subunits [24,25], promoting an activation mechanism independent of Thr172 phosphorylation. Indeed, binding of A-769662 can increase the AMPK activity >90-fold when Ser108 in the CBM domain of the β-subunit is phosphorylated [26], and may also protect against dephosphorylation of Thr172 [21].

Several direct AMPK activators have been reported in the last few years, showing in some cases a marked isoform selectivity, [27] as can be noticed upon inspection of the biochemical data collected in Table 1 for selected small molecule AMPK activators. A-769662 is active in α2β1γ1 but not in α2β2γ1, at least up to concentrations of 10 μM [24], demonstrating selectivity toward β1-containing AMPK complexes. Likewise, the enzyme activation is ~7-fold larger in α2β1γ1 relative to α2β2γ1. A mild β1-selective activation is found for 991 and SC4, as they activate β1- and β2-containing AMPK complexes, although a higher (~2-fold) activation is observed in the former case [24,28,29]. The activation also seems to be slightly larger for the enzyme containing the α2 isoform. While PF-249 is an activator selective for β1-containing complexes, PF-739 is a pan-activator that activates α2β1γ1 and α2β2γ1 complexes, though it still exhibits a larger affinity for the β1-containing isoforms (EC_{50} ratio of ~ 8 and ~ 15 between α2β1γ1/α2β2γ1 and α1β1γ1/α1β2γ1, respectively) [30]. PF-739 seems also to have a larger effect on the α2-containing AMPK complexes, as the ratio of the EC_{50} values is 1.8–3.2 larger for α1β1γ1 and α1β2γ1 relative to the α2-containing enzymes. Finally, MT47-100, a structural analogue of A-769662 possessing a dihydroquinoline ring instead of the thienopyridone core, activates both α1β1γ1 and α2β1γ1, but promotes the inhibition of β2-containing complexes [31].

Understanding the molecular mechanisms that underlie the regulatory effect of direct activators, particularly targeting selectively a given isoform, is of utmost relevance for gaining insight into the puzzling tissue-dependent modulation of AMPK, and to disclose drugs active against specific pathological disorders. Given the sensitivity of the AMPK enzyme to the precise combination of different isoforms, as exemplified by the distinctive trends observed in the activation of complexes with α1/α2 and β1/β2 isoforms (see above), we have adopted a 'divide-and-conquer' strategy in order to explore the molecular basis of the selective isoform activation of AMPK, specifically focusing on the role played by β1- and β2-subunits. To this end, extended molecular dynamics (MD) simulations have been performed for the apo forms, the holo complexes formed with A-769662 and SC4 bound to the ADaM site, and the ternary (holo + ATP) complexes formed by the enzyme bound to both activator (in the ADaM site) and ATP (in the ATP-binding site). The analysis of the structural and dynamical properties of AMPK complexes and the identification of the interaction networks between α- and β-subunits have unveiled distinctive molecular determinants of the allosteric regulation exerted by direct activators on β1- and β2-containing enzymes.

2. Material and methods

2.1. Molecular dynamics simulations

Extended molecular dynamics (MD) simulations were utilized to analyze the structural and dynamical characteristics of the simulated system. For this purpose, the α2β1γ1 systems were built up using the complexes with A-769662 (PDB entry 4CFF) [24] and SC4 (PDB entry 6B1U) [29]. On the other hand, the system related to the complex of α2β2γ1 bound to SC4 (PDB entry 6B2E) [29] was also used as a template to model the complexes with A-769662. Following our previous studies [32], the γ-subunit was not considered in MD simulations due to several reasons. First, the ADaM site is shaped only by α- and β-isoforms. Furthermore, the lack of precise structural information about stretches of both α- and β-subunits, particularly regarding the C-terminal regions, which are located close to the γ-subunit, would introduce an additional level of uncertainty, opening the way to potential artefacts in the simulations. Finally, inclusion of the γ-subunit would have required a larger computational cost in order to guarantee a proper sampling of the dynamical motions of the three isoforms. Accordingly, following the 'divide-and-conquer' strategy outlined above, the simulated systems comprise only α- and β-subunits. Specifically, simulations were performed for residues 8–278 of the α2 isoform, and residues 78–173 and 77–171 of the β1- and β2-isoforms, which were solved without disruptions in the X-ray structures. Finally, these structures were used to model the apo protein, the complexes of the activators bound to the phosphorylated Ser108 (pSer108)-containing isoforms (holo), and the corresponding holo + ATP complexes with both activator in the ADaM site and ATP in the ATP-binding site.

Simulations were performed using the AMBER18 package [33] and the Amber ff99SB-ILDN force field [34] for the protein, whereas the ligands (A-769662, SC4) were parameterized using the GAFF [35] force field in conjunction with restrained electrostatic potential-fitted (RESP) partial atomic charges derived from B3LYP/6-31G(d) calculations [36]. The standard protonation state at physiological pH was assigned to ionisable residues, and a capping group (N-methyl) was added to the C-terminus of the α-subunit. The simulated systems were immersed in an octahedral box of TIP3P water molecules [37]. Counterions atoms were added to maintain the neutrality of the simulated systems [38]. The final systems included the AMPK protein, around 25,000–28,000 water molecules, and a variable number of Na^+ and Cl^- ions, leading to simulated systems that contain between 81,000–90,000 atoms (specific details are given in Table S1).

Simulations were performed in the NPT ensemble for equilibration and NVT for MD productions using periodic boundary conditions and Ewald sums (grid spacing 1 Å) for treating long-range electrostatic interactions. Apo, holo and holo + ATP systems were simulated in triplicate. The minimization of the systems was performed refining the position of hydrogen atoms in the protein (2000 cycles of steepest descent algorithm followed by 8000 cycles of conjugate gradient), subsequently minimizing the position of water molecules (using again the previous scheme), and finally minimization of the whole system (4000 cycles for steepest descent and 1000 cycles of conjugate gradient). Later, the temperature of the system was gradually raised from 100 to 300 K in 5 steps, 50 ps each using the NVT ensemble. In this process, suitable restraints (5 kcal mol^{-1} $Å^{-2}$) were imposed to keep the ligand (activator, ATP) in the binding pocket and prevent artefactual rearrangements along the equilibration stage. In order to equilibrate

Table 1
Activation of AMPK isoforms by selected direct activators.

Activator	Property [a]	Isoform			
		α2β1γ1	α2β2γ1	α1β1γ1	α1β2γ1
A-769662					
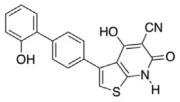	Activation fold [b]	14.3	NA [c]	2.0	NA [c]
	K_d (μM) [b]	0.40	–	0.51	14.5
991					
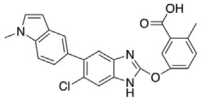	Activation fold [b]	12.2	5.4	4.8	2.4
	K_d (μM) [b]	7.7 [d,e]	5.7 [d]		
		0.06[f]	–	0.06	0.51
		0.085		0.078	1.18
SC4					
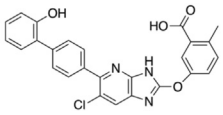	Activation fold [g]	5.2	2.9	2.4	1.2
	EC_{50} (nM) [g]	–	17.2	5.1	–
PF-249					
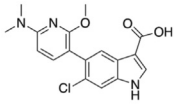	EC_{50} (nM) [h]	8.04	> 40 μM	9.37	> 40 μM
PF-739					
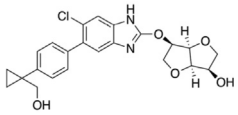	EC_{50} (nM) [h]	5.23	42.4	8.99	136
MT47-100					
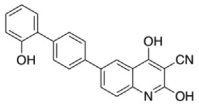	Activation fold [i]	2.3	0.5	2.5	0.4

[a] Activation fold measured relative to the basal activity of the enzyme. Dashed lines stand for systems were no experimental data have been reported, to the best of our knowledge. [b] Ref 24. [c] No activation detected up to a concentration of 10 μM. [d] Ref. 28. [e] Determined for α2β1γ2. [f] Values obtained by using either biolayer interferometry or circular dichroism. [g] Ref. 29. [h] Ref. 30. [i] Ref. 31.

the density of the system an additional 5 ns step performed in the NPT ensemble. In addition, the restraints were progressively eliminated in this later step. Production MD simulations were run for 1 μs per replica, leading to a total simulation time of 24 μs for the ligand-bound AMPK complexes, and 6 μs for the two apo species of AMPK.

2.2. Essential dynamics

This method was utilized to specify the most important motions from the structural variance sampled in MD simulations. In essential dynamics (ED) [39], the dynamics along the individual modes can be studied and visualized separately, so we can filter the main collective motions during our simulations. Therefore, the positional covariance matrix is created and diagonalized in order to achieve the collective deformation modes, i.e. the eigenvectors, while the eigenvalues account for the contribution of each motion to the structural variance of the protein. ED analysis was done for 25,000 snapshots from the last 500 ns of each simulation, taking into account only the backbone atoms and the calculations were performed with PCAsuite program (available at http://www.mmb.irbbarcelona.org/software/pcasuite/pcasuite.html), which is integrated in the pyPCcazip program, a suite of tools for compression and analysis of molecular simulations [40].

2.3. Conformational entropy

The quasi-harmonic approximation proposed by Schlitter [41] was used to calculate the conformational entropy sampled for the different simulation systems. Due to the sensitivity of these calculations to simulation time and sampling [42], the conformational entropy determined at regular interval times ($S(t)$) along the MD simulation was used to estimate the conformational entropy at infinite time (S^{∞}) [43]. In particular, $S^{\infty}$was determined by fitting the asymptotic behaviour of the curve according to the expression $S(t) = S^{\infty}\frac{t}{t+\alpha}$, where α is an adjustable parameter by curve fitting. In order to enable a direct comparison between the conformational entropies of the different α2β1 and α2β2 systems, only the set of atoms of the protein backbone were considered in entropy calculations, thus avoiding a bias originated from the residue substitutions between β1- and β2-isoforms in the calculated entropies (note that a different choice of atoms, including both backbone and side chains, was used in the comparison of the conformational entropies reported for α2β1 bound to A-769662 in a previous study [32]).

2.4. Dynamical cross-correlation analysis

To complement the information gained from the ED analysis, dynamical cross-correlation (DCC) was used to examine the corre-

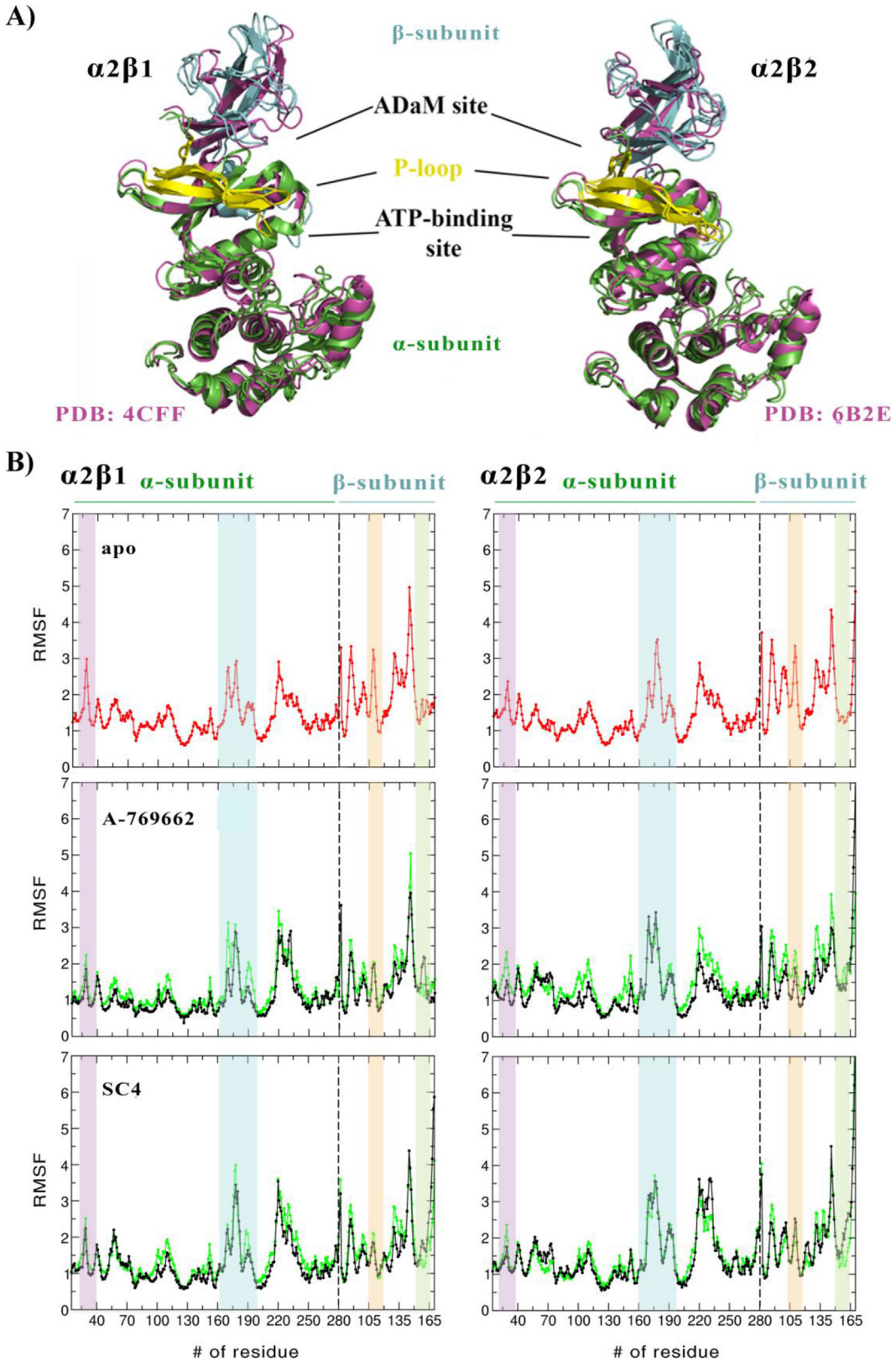

Fig. 1. A) Superposition of the energy-minimized averaged holo + ATP structures for α2β1 and α2β2 complexes with A-769662 and SC4 (ligands are not shown for the sake of clarity). The backbone of α and β subunits is shown as green and blue cartoon, respectively (P-loop highlighted in yellow). The X-ray structures of α2β1 and α2β2 (PDB IDs 4CFF and 6B2E, respectively) are shown in magenta cartoon. B) RMSF (Å) average of the residues determined along the last 500 ns of the three independent replicas run for apo (red), holo and holo + ATP (green and black, respectively). Complexes bound to A-769662 and SC4 are shown in *middle* and *bottom* panels. The highlighted bars denote regions corresponding to P-loop (purple), activation loop (cyan), CBM domain (orange), and C-interacting helix (green). (For interpretation of the references to colour in this figure legend, the reader is referred to the web version of this article.)

lation motion of residues along a given trajectory. To this end, all the snapshots were aligned by means of least-square fitting of C_α atoms of the whole protein to the equilibrated starting configuration. Then, the DCC matrix was determined as noted in Eq. (1).

$$C_{ij} = \frac{c_{ij}}{c_{ii}^{1/2} c_{jj}^{1/2}} = \frac{\langle r_i r_j \rangle - \langle r_i \rangle \langle r_j \rangle}{\left[\left(\langle r_i^2 \rangle \langle r_i \rangle^2 \right) \left(\langle r_j^2 \rangle - \langle r_j \rangle^2 \right) \right]^{1/2}} \quad (1)$$

where the position vectors of two C_α atoms i and j fitted in the structure at time t are denoted as $\mathbf{r}_i(t)$ and $\mathbf{r}_j(t)$, respectively.

The cross-correlation coefficients range from −1 to + 1, which represent anticorrelated and correlated motions, respectively, whereas values close to zero indicate the absence of correlated motions [44]. This analysis was performed using the module available in AMBER package. The similarity between the DCC matrices computed for the three replicas run for apo, holo and holo + ATP systems was estimated using the Tanimoto similarity index [45]. This parameter is a distance metrics used to quantify the degree of similarity between two sets of data. While this index is widely adopted to compare the descriptors that characterize the chemical structure of molecules, in this study it is used to compare the correlated motions determined for pairs of residues in the AMPK complexes.

2.5. Interaction energy network

Networks of local interactions are intrinsically linked to the structural response of proteins to external factors [46]. For our purposes, Weighted Implementation of Suboptimal Path (WISP) [47] was utilized to analyze the allosteric network. This method enabled us to perform a dynamic network analysis to understand how the binding of a ligand in an allosteric cavity could affect another binding site. In particular, WISP relies on the dynamical interdependence among the protein residues. To this end, each amino acid is treated as a node, which was located at the residue center-of-mass, and the interdependence among nodes is represented as a connecting edge with an associated numeric value that reflects its strength. The interdependence is determined from an *NxN* matrix *C* (*N* is the number of nodes) with values corresponding to the weights of each edge, reflecting the correlated motion among node–node pairs. Finally, the weight between the edge that connects nodes i and j is expressed as $w_{ij} = -\log(|C_{ij}|)$, so that highly correlated or anticorrelated motions are characterized by small values of w_{ij}. This analysis was performed for the last 500 ns of the MD simulations.

3. Results

MD simulations were performed to examine the structural and dynamical changes triggered by A-769662 and SC4 through the analysis of the apo form of AMPK considering both α2β1 and α2β2 isoforms, and their holo and holo + ATP complexes, as well as the interaction networks implicated in the dynamical response to activator binding. Three independent replicas (1 μs/replica) were run for each system, leading to a total simulation time of 6 μs for the apo species and 24 μs for the ligand-bound complexes.

3.1. Global structural analysis of AMPK complexes

The effect of activator and ATP binding on the structural features of AMPK complexes was examined from the positional root-mean square deviation (RMSD) of the protein backbone along the simulation. The average structure of the holo + ATP species sampled in the last 200 ns of the three simulations run for each activator was used as reference. There is a large structural resemblance between the averaged holo + ATP species, as noted in the superposition of the protein backbone for the complexes of α2β1 (Fig. 1A left) and α2β2 (Fig. 1A right) bound to ATP and either A-769662 or SC4. The structural resemblance of the energy-minimized averaged holo + ATP structures is also noted in RMSD values of 0.8–1.6 Å, which supports the preservation of the overall fold of the protein upon binding of both activator and ATP. Preservation of the overall structure of holo + ATP complexes is also supported by the small fluctuations observed in RMSD profiles (Fig. S1 and S2), as noted by the values of 1.9–2.3 Å for α2β1 and 1.9–2.7 Å for α2β2 (Table 2). For the α2β1 systems, the RMSD of the sampled structures is reduced from apo (2.5–3.2 Å) to holo (1.9–2.9 Å) to holo + ATP (1.9–2.3 Å), revealing that binding of activator and ATP stabilizes the overall fold of the complex (Table 2). This effect is less apparent for the α2β2 complexes, as the RMSD values of the apo species (2.7–3.9 Å) are similar or even lower than those determined for the holo form (2.9–4.5 Å), suggesting that the activator exerts a weaker structural stabilization upon binding to α2β2 isoform.

On the other hand, the per-residue mean square fluctuation (RMSF) profile is similar for the two isoforms, as noted in the resemblance of the fluctuation pattern obtained by averaging the RMSF of the three replicas run for every system (Fig. 1B). The highest fluctuations in the α-subunit mainly originate from residues in the activation loop (residues 165–185) and the α-helix between residues 210–230. The largest fluctuations in the β-subunit correspond to residues in the CBM domain, which contains Ser108, and regions proximal to the C-interacting helix. Compared to the

Table 2
RMSD and standard deviation (Å) determined for the protein backbone of the snapshots sampled along the last 500 ns of MD simulations performed for all systems (apo, holo and holo + ATP states of AMPK isoforms α2β1 and α2β2). Values were determined using the energy-minimized holo + ATP species averaged for the last 200 ns of each simulation system as reference structure.

Activator	System	Replica 1	Replica 2	Replica 3	Average
α2β1					
A-769662	**apo**	2.5 ± 0.5	3.1 ± 0.6	2.6 ± 0.3	2.7
	holo	2.3 ± 0.4	1.9 ± 0.3	2.2 ± 0.3	2.1
	holo + ATP	1.9 ± 0.2	2.0 ± 0.3	1.9 ± 0.2	1.9
SC4	**apo**	3.2 ± 0.5	2.9 ± 0.5	3.1 ± 0.4	3.1
	holo	2.9 ± 0.4	2.2 ± 0.3	2.3 ± 0.6	2.5
	holo + ATP	2.0 ± 0.2	2.3 ± 0.2	2.2 ± 0.2	2.2
α2β2					
A-769662	**apo**	2.7 ± 0.3	3.3 ± 0.3	3.9 ± 0.4	3.3
	holo	4.2 ± 0.5	3.2 ± 0.4	4.5 ± 0.4	4.0
	holo + ATP	2.1 ± 0.2	2.2 ± 0.2	1.9 ± 0.1	2.1
SC4	**apo**	3.0 ± 0.3	2.8 ± 0.2	3.4 ± 0.4	3.1
	holo	3.3 ± 0.3	2.9 ± 0.3	3.1 ± 0.3	3.1
	holo + ATP	2.3 ± 0.2	2.5 ± 0.2	2.7 ± 0.2	2.5

apo forms, binding of activators generally lead to subtle changes in the RMSF profile, such as enhanced fluctuations in the activation loop, and the α-helix mentioned above, while a reduction in the fluctuation of residues in the β-subunit is observed. In contrast, the RMSF profiles remain generally unaltered upon subsequent binding of ATP, as noted in the comparison of the results obtained for holo and holo + ATP systems.

3.2. Dynamics of AMPK complexes

The dynamical behavior of proteins exerts a major role in their function at multiple time scales, affecting processes such as enzyme catalysis [48–50]. Here the effect of activator on the dynamics of AMPK was examined by analyzing the essential dynamics (ED) and conformational entropy of the protein back-

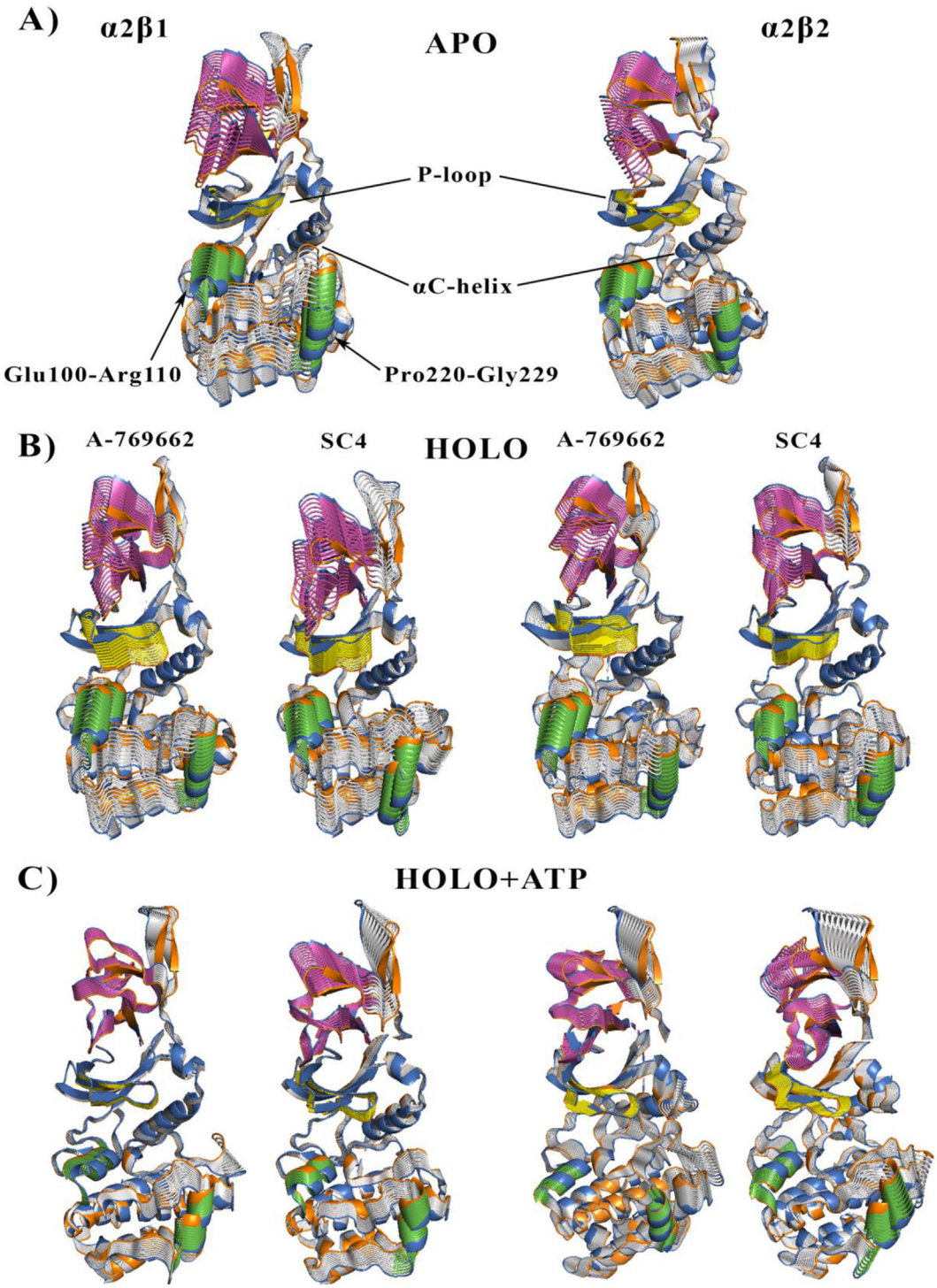

Fig. 2. Representation of the first essential motion derived from the ED analysis of the protein backbone for A) the α2β1 and α2β2 apo species, and their B) holo and C) holo + ATP complexes with A-769662 and SC4 determined from the snapshots sampled along the last 500 ns of simulations. The P-loop is shown in yellow, the helices formed by residues 100–110 and 220–229 in the α-subunit in green, and the CBM domain in magenta. (For interpretation of the references to colour in this figure legend, the reader is referred to the web version of this article.)

bone in conjunction with the cross-correlation mapping at the residue level.

ED was used to characterize the effect of ligand binding on the major motions of the protein backbone. For the two apo species, the first essential motion involves a concerted bending that brings the core of α-helices in the α-subunit and the β-sheets in the β-subunit closer and then moves them apart (Fig. 2A). Nevertheless, there are slight differences in the extent of this motion for certain structural elements, such as the deformation of the CBM unit and the P-loop, which is located at the interface of ADaM and ATP-binding sites (Fig. S3). On average, the first motion accounts for 41% of the structural variance in α2β1, and 31% in α2β2. The difference in the conformational variance observed in the first essential motion is also reflected in the cumulative variance explained by the three main essential motions, which amounts to 66% and 57% of the structural flexibility in α2β1 and α2β2, respectively (Fig. S4). This highlights the significant contribution of the first essential motion to the conformational flexibility of the AMPK complexes. On the other hand, the conformational entropy of the two apo forms is basically the same (~19 kcal K^{-1} mol^{-1}; Table 3).

Binding of activator and ATP reduces the conformational variance originated from the first three essential motions in α2β1 complexes with A-769662 and SC4 (from 66% to 58% to 47% from apo to holo to holo + ATP in the case of A-769662), reflecting the trend observed for the first essential motion (Fig. S4). This leads to a progressive decrease in the conformational entropy of the protein skeleton (Table 3). In contrast to the apo species, the activator promotes the synchronous motion of the P-loop and the CBM domain, which bends toward the α-subunit (Fig. 2 and S5). Subsequent binding of ATP in the kinase domain, however, reduces the overall flexibility of the protein, especially regarding the P-loop and most of the helices in the α-subunit, but also elements of the β-subunit proximal to the ADaM site, reflecting the synergy between activator and ATP in increasing the stiffness of the AMPK complex.

The dynamical behaviour observed for α2β1 is less regular in α2β2. Thus, the structural variance explained by the first essential motion in the apo form remains unaltered or is even slightly increased in the presence of the activator (Fig. S4). Furthermore, although the activator increases the conformational flexibility of the P-loop, the response of other structural elements is more variable, as noted for instance in the deformations observed for certain helices in the α-subunit, such as those formed by residues Glu100-Arg110 and Pro220-Gly229, or the β-sheets in the N-terminus of the β-subunit (Fig. 2 and S5), this effect being generally more pronounced for SC4-bound complexes. The lack of a uniform, consistent pattern of structural flexibility is also found in the holo + ATP systems, as well as in the distinct changes observed in the conformational entropy for A-769662 and SC4 (Table 3).

To complement the preceding results, dynamical cross-correlation (DCC) analysis was performed to examine the correlated motions of residues in AMPK complexes. Results for α2β1 and α2β2 complexes interacting with A-769662 are shown in Fig. 3. The overall trends are similar to those obtained for the SC4-bound systems (Fig. S6). Binding of activator and ATP promotes a general decrease in the dynamical correlation of residues. This is reflected in the weakening of the correlated regions in the DCC map (Fig. 3B-C and S6B-C), as one may notice a progressive reduction in the number and intensity of the areas that exhibit a pronounced correlation (shown in yellow and blue for highly correlated and anticorrelated fluctuations between residues in plots B and C, which correspond to holo and holo + ATP species). Furthermore, one may note that this effect is more noticeable for the α2β1 isoform. The apo systems (Fig. 3A and S6A) exhibit a correlation between the P-loop, the α-helix formed by residues 100–110 and the αC-helix (as noted by the yellow marks), which pertain to the α-subunit. In turn, they are correlated with the C-interacting helix in the β-subunit. Binding of activator and ATP reinforces the correlation between the motion of the CBM domain and the P-loop (black square in Fig. 3 and S6). This effect is more pronounced for the α2β1 isoform, which shows a more consistent dynamical response to activator binding, as noted in similarity indexes of 0.91 (A-769662) and 0.84 (SC4) obtained from the comparison of DCC matrices derived for the simulations of α2β1 (Table S2), whereas the similarity is reduced to 0.75 for α2β2. Remarkably, this difference is even larger for the dynamical coupling between α- and β-subunits, as noted in similarity indexes of 0.89 (A-769662) and 0.83 (SC4) for α2β1, which are reduced to 0.59 and 0.66 for α2β2, respectively.

Despite the overall gross similarity in the dynamical behavior of both α2β1 and α2β2 isoforms, the preceding results reveal the occurrence of subtle differences between β1- and β2-containing AMPK complexes. In particular, the results suggest that the α2β2 complex has a larger resilience to the structural modulation exerted by the activator, whereas the α2β1 isoform is more sensitive to the conformational adaptation induced upon activator binding to the ADaM site, enhancing the stiffness of protein backbone for the β1-containing complex, especially for A-769662.

3.3. Pre-organization of the ATP-binding site

To examine the implications of the differences in the dynamical response to binding of activator, we determined the structural resemblance of the ATP-binding site along the simulations obtained for apo, holo, and holo + ATP systems. To this end, we decided to use the average structure of the holo + ATP complex as reference, this choice being motivated by two major reasons: i) the large structural resemblance of the energy-minimized averaged holo + ATP structures for α2β1 and α2β2 complexes with A-769662 and SC4 (see Fig. 1A), and ii) the notable reduction in the conformational flexibility of the ATP binding site for the holo + ATP species (see plots C in Fig. 2).

For the holo + ATP species, the residues in the ATP-binding site sample a reduced conformational space, with a peak generally centred at a positional RMSD of 1.0–1.6 Å for α2β1 and α2β2 isoforms (Fig. 4). In contrast, the apo form exhibits a wider distribution, showing either a single or a bimodal RMSD profile, with values ranging from 1.0 to 5.5 Å. This reflects that the ATP-binding site in the apo species is more conformationally mobile than in the holo + ATP state. Due to this conformational flexibility, the ATP-binding site can often adopt conformations close to those populated in the holo + ATP state, but also visit more dissimilar conformational regions. The most distinctive features emerge from the

Table 3
Entropy values at infinite simulation time (S^{∞}; kcal K^{-1} mol^{-1}) determined for the protein backbone of apo, holo and holo + ATP systems of AMPK. Changes in conformational entropy (ΔS^{∞}) are determined relative to the apo species. Values averaged for the three independent simulations run for the systems (standard deviation in parenthesis).

Species	α2β1	α2β2
S^{∞}**(apo)**	19.1 (0.2)	18.8 (0.3)
A-769662		
S^{∞}**(holo)**	18.9 (0.1)	18.6 (0.2)
ΔS^{∞}**(holo)**	−0.2	−0.2
S^{∞}**(holo + ATP)**	18.5 (0.1)	18.4 (0.1)
ΔS^{∞}**(holo + ATP)**	−0.6	−0.4
SC4		
S^{∞}**(holo)**	18.8 (0.4)	19.0 (0.2)
ΔS^{∞}**(holo)**	−0.3	+0.2
S^{∞}**(holo + ATP)**	18.5 (0.3)	19.0 (0.6)
ΔS^{∞}**(holo + ATP)**	−0.6	+0.2

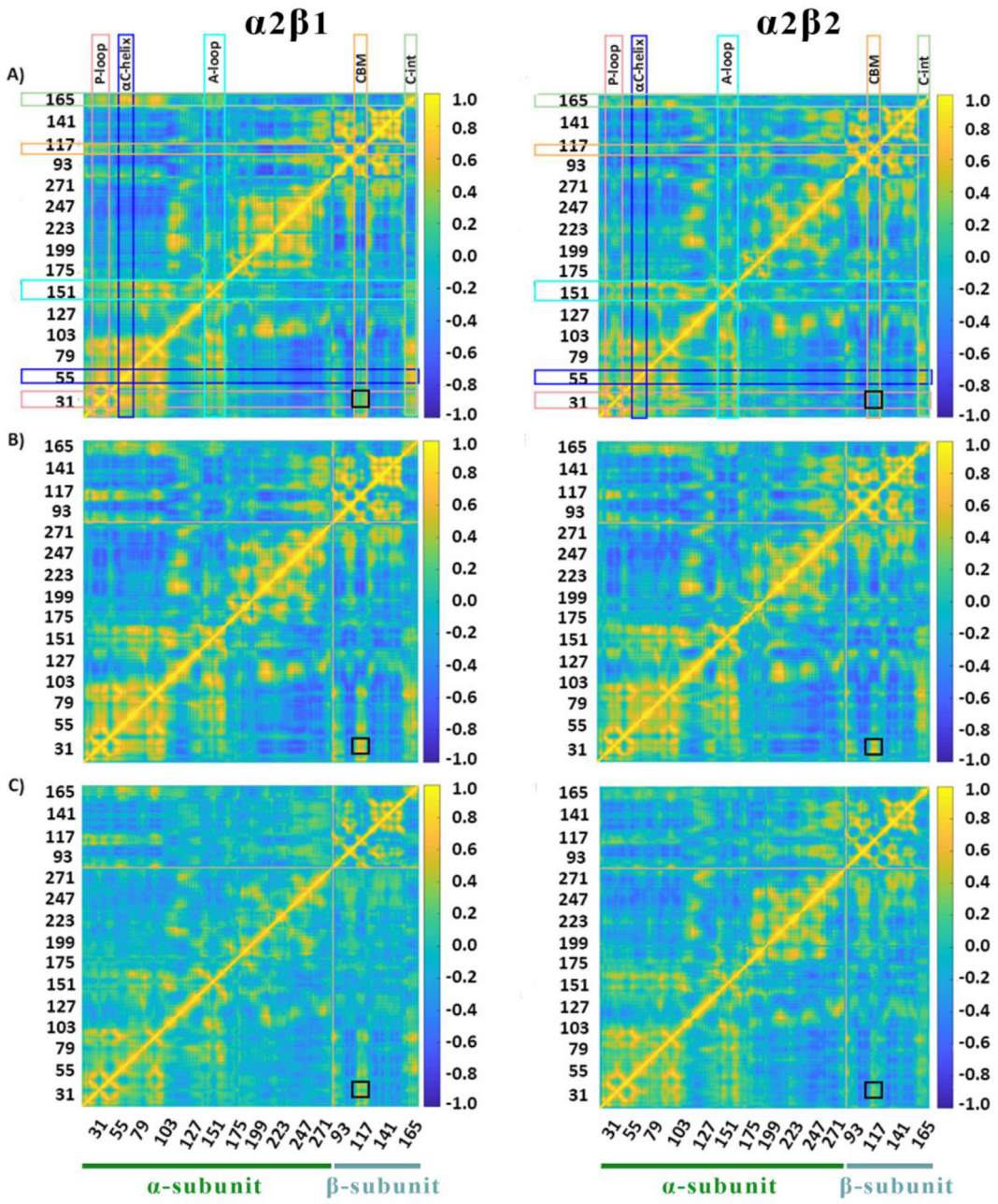

Fig. 3. Dynamic cross-correlation (DCC) matrices for A) apo, B) holo and C) holo + ATP complexes of (left) α2β1 and (right) α2β2 with A-769662. The x- and y-axis denote the numbering of residue in the α- and β-subunit. The residues pertaining to the α- and β-subunits are indicated at the bottom of the plot (green and blue lanes for α- and β-subunits, respectively). Specific regions of AMPK are highlighted with squares at the top of the plot: P-loop (pink), αC-helix (blue), activation loop (A-loop; cyan), CBM unit (orange) and C-interacting helix (C-int; green). Regions colored in yellow/blue show high correlated/anticorrelated fluctuations. The black square in the plots highlights the motion between the CBM domain and the P-loop. (For interpretation of the references to colour in this figure legend, the reader is referred to the web version of this article.)

distribution profiles of the holo species. For the α2β1 complexes, binding of the activator shifts the holo distribution toward the holo + ATP profile. This is clearly observed in the complexes with A-769662, where the peak in the apo distribution located at 2.8 Å is shifted to 1.5 Å for the holo species, and SC4, where the broad distribution observed for the apo species is converted into a narrower band that matches well the distribution of the holo + ATP system (Fig. 4). In contrast, the RMSD profile obtained for α2β2 complexes reveals that the activator leads to structures where the ATP-binding site has less resemblance to the holo + ATP system (Fig. 4). The analysis of the distinct structural elements that shape the ATP-binding site shows that the differences observed for α2β1 and α2β2 holo species mainly arise from the conformational changes of the P-loop rather than from residues in the helical domain of the α-subunit (data not shown), suggesting that the activator is more effective in inducing the remodeling of the P-loop toward active-like conformations in β1-containing complexes.

These results are in agreement with the larger activation exerted by A-769662 for the α2β1 isoform, while a weaker effect is observed for α2β2 isoform (Table 1), supporting the hypothesis that the activator acts as a molecular glue in α2β1 that connects the fluctuations of the CBM domain in the β-subunit with the P-loop, facilitating the arrangement of key structural elements, particularly the P-loop, toward conformations favouring the binding of ATP. These trends can be extrapolated to SC4, although the

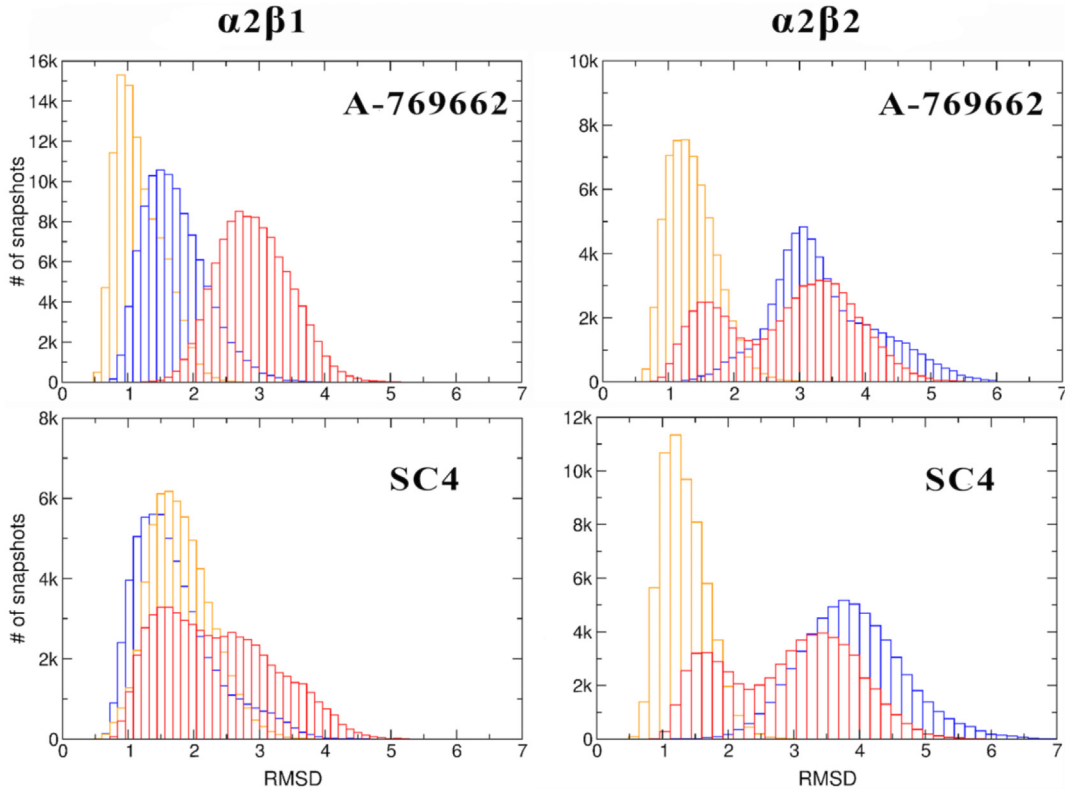

Fig. 4. Distribution of the positional deviation (RMSD; Å) of the structures sampled along the trajectories run for apo (red), holo (blue), and holo + ATP (orange) for the residues that shape the ATP-binding site (residues α22–α32, α42–α46, α75–α79, α142–α147, and α153–α157). A total of 60,000 snapshots taken from the last 500 ns of MD simulations were considered for each system in the analysis. (For interpretation of the references to colour in this figure legend, the reader is referred to the web version of this article.)

difference between α2β1 and α2β2 is less apparent compared to A-769662 (Table 1).

3.4. Structural basis of the selective β1-containing AMPK activation by A-769662 and SC4

Accordingly, to explore the structural basis of the selective activation of β1-containing AMPK by A-769662, we examined the network of interactions formed between the activator with both P-loop and CBM unit, paying attention to the occurrence of residue substitutions between β1- and β2-isoforms (Fig. S7).

At the inner edge of the ADaM site in holo α2β1, βArg83 consistently forms a salt bridge with αAsp88 (average distance of 3.2 ± 0.2 Å from the guanidinium unit to the carboxylate group), which is assisted by a hydrogen bond between αAsp88 and the thienopyridone ring of A-769662 (2.8 ± 0.2 Å; Fig. 5A). At the outer edge of the ADaM site, the phosphorylated βSer108 (βSer108p) adopts two arrangements that enable interactions with αLys31 (4.3 ± 1.4 Å) and αLys29 (3.5 ± 0.8 Å). Binding of A-769662 is also assisted by hydrophobic contacts of the ligand with αVal11, αLeu18, αIle46, αPhe90 and βVal113 (not shown in Fig. 5A for the sake of clarity in the graphical display), forming a tightly packed cage around A-769662.

This interaction pattern is drastically altered in holo α2β2, as noticed in the loss of the β2Arg82-αAsp88 interaction (N…O distance > 7.1 Å; Fig. 5B). This can be attributed to the replacement β1Asn111 → β2Asp111, as this latter residue competes with αAsp88 in forming electrostatic interactions with β2Arg82. In fact, β2Arg82 adopts a distinct conformation that enables a direct salt bridge with βSer108p, which maintains a fixed orientation in contrast to the dual arrangement found in holo α2β1. This weakens the role of A-769662 in mediating the interaction between the CBM domain and the P-loop. Indeed, the impact of the β1Asn111 → β2Asp111 change is reflected in the major interaction pathways identified from WISP analysis for the two holo species. In holo α2β1, the CBM domain and the P-loop are connected via three pathways, implying in one case the passage through βSer108p, and the involvement of the ligand, especially via the triad βArg83-αAsp88-A-769662, in the other two (Fig. 5C; close up view shown in Fig. S8). In contrast, only the βSer108p pathway is found in holo α2β2, which suggests a weaker ability of A-769662 to act as a gluing molecule between the β2-subunit and the P-loop compared to holo α2β1 (Fig. 5D; see also Fig. S8).

Compared to A-769662, SC4 exhibits a mild preference for activation of β1-containing AMPK (Table 1), raising questions about the interaction network formed by SC4 in the holo species. The analysis reveals a more complex scenario, since two arrangements are found for βArg83 (βArg82) in holo α2β1 (α2β2) (Fig. 6A-B). In one case, βArg83 (βArg82) forms a salt bridge with αAsp88 (3.1 ± 0.2 Å), which also accepts a hydrogen bond from the imidazo[4,5-b]pyridine ring of SC4 (3.4 ± 0.2 Å), whereas αLys29 interacts with βSer108p (3.3 ± 0.7 Å) and is hydrogen bonded with the pyridine-like/imidazole-like nitrogen atoms of SC4 (3.6 ± 0.6 Å, Fig. 6A-B, residues in cyan). Alternatively, βArg83 (βArg82) interacts with βSer108p (Fig. 6A-B, residues in grey), forming an additional cation-π interaction with the imidazo[4,5-b]pyridine ring, which in turn is hydrogen bonded to αLys29. Remarkably, in holo α2β2 this latter arrangement of βArg82 is also stabilized by the interaction with βAsp111.

In contrast to A-769662, the occurrence of this dual interaction pattern reflects the electrostatic influence of the carboxylate group present in SC4, which would facilitate the adoption of the two

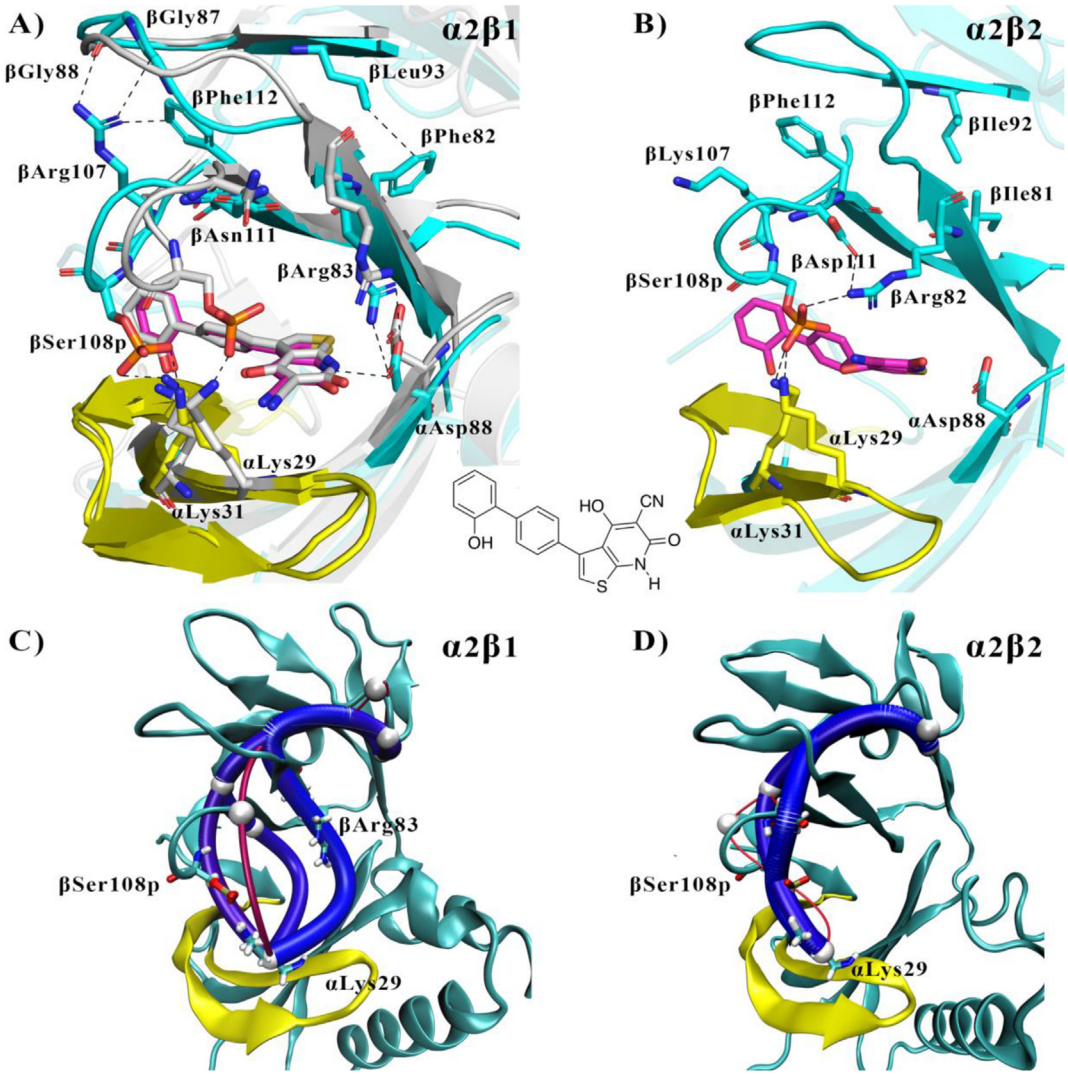

Fig. 5. Representation of selected interactions between the CBM, P-loop and A-769662 in holo A) α2β1 and B) α2β2. The two arrangements of βSer108p in holo α2β1 are shown in cyan and grey colors (P-loop in yellow). A-769662 is shown as coloured (carbon atoms in magenta) sticks in the ADaM site, and a 2D representation of the chemical structure is shown for the sake of clarity. Selected interactions between residues are highlighted as dashed lines. Major interaction networks obtained from WISP analysis for C) α2β1 and D) α2β2 systems (close up views available in Fig. S8). (For interpretation of the references to colour in this figure legend, the reader is referred to the web version of this article.)

arrangements of βArg83 (βArg82). When βArg83 forms a salt bridge with αAsp88 in holo α2β1, the CBM unit and the P-loop are then connected by two main pathways, which reveal the involvement of either βSer108p or the triad βArg83-SC4-αLys29 (Fig. 6C left; close up view shown in Fig. S8). However, when the βArg83-αAsp88 salt bridge is lost (Fig. 6C right, and Fig. S8), the CBM and P-loop are linked via βAsn111, the phosphate unit of βSer108p and αLys31 as well as via direct interactions between βArg83 and the βSer108p phosphate unit. The interaction network observed in holo α2β2 exhibits a more diverse pattern, likely reflecting the larger flexibility observed in this species relative to holo α2β1. Thus, besides the βArg82-SC4-αLys29 triad, which defines the main pathway, an alternate network involves the correlated motion of the pair formed by αLys29 and the βSer108p phosphate unit, whereas the loss of the βArg82-αAsp88 salt bridge primarily reinforces the connection via βSer108p, which is also assisted by another path where βArg82 interacts with both βAsp111 and the βSer108p phosphate group. Compared to the behavior found for A-769662 bound to α2β1 and α2β2 (Fig. 5C and D), these findings provide a basis to understand the mild selectivity of SC4 between α2β1 and α2β2 isoforms.

4. Discussion and conclusion

Unveiling the molecular factors that underlie the structure–function relationships of AMPK isoforms is necessary to rationalize the tissue-dependent expression of AMPK complexes, enabling the design of tailored compounds active against specific metabolic disorders. This question, however, is challenged by the high structural and dynamical behavior observed for α2β1 and α2β2 complexes, although our results have revealed subtle differences in the dynamical response of AMPK to the binding of activators, showing a larger mechanical sensitivity of the α2β1 complex and a larger resilience of the α2β2 species, especially regarding modulation by A-769662.

The different interaction networks observed upon binding of A-769662 to α2β1 supports the effective role of the activator in assisting synergistically the fluctuations of the CBM unit and the P-loop, facilitating the adoption of pre-organized conformations that favor the binding of ATP, shifting the enzyme towards an active state. This effect is weakened in holo α2β2, which results in decreased efficacy of A-769662 in acting as a molecular glue between the CBM unit and the P-loop, making the enzyme less

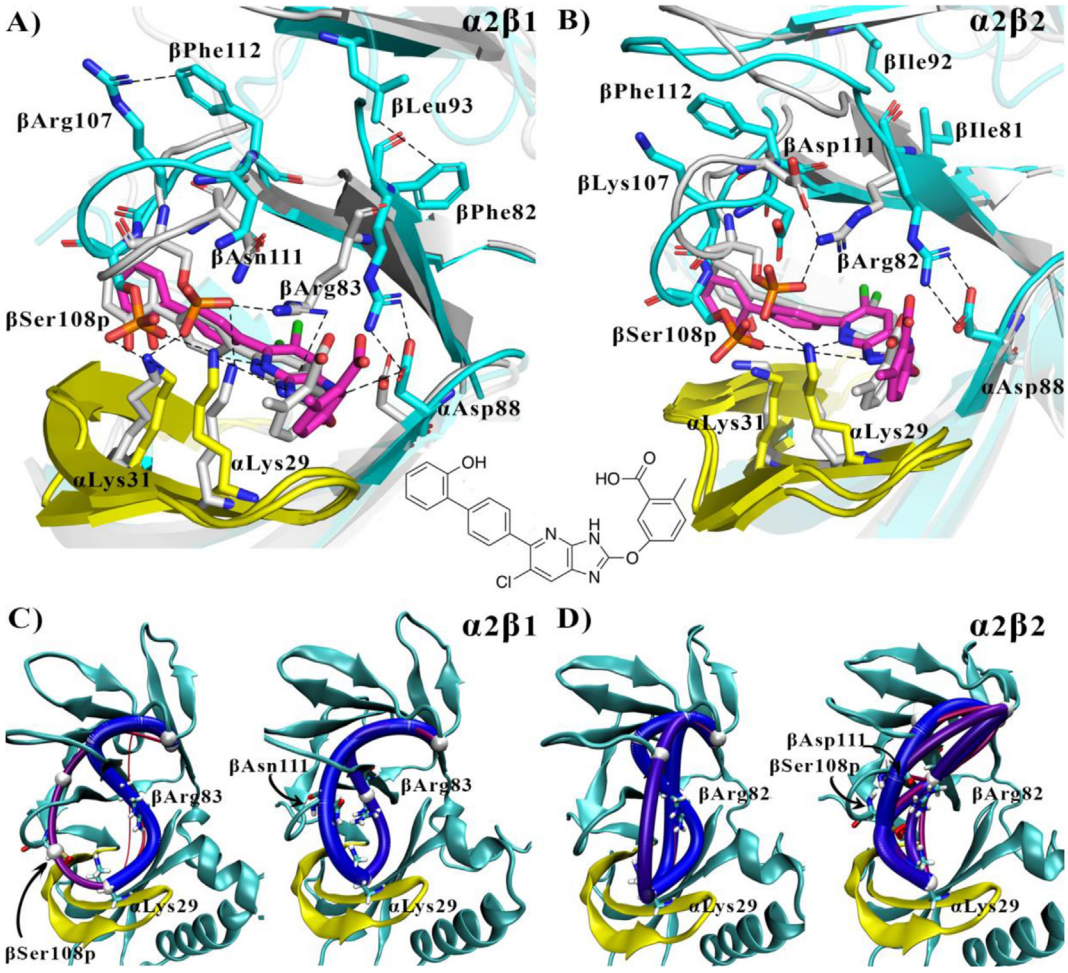

Fig. 6. Representation of selected interactions between the CBM, P-loop and SC4 in holo A) α2β1 and B) α2β2. The distinct conformational arrangements are shown in cyan and grey colors (P-loop in yellow). SC4 is shown as coloured (carbon atoms in orange) sticks in the ADaM site, and a 2D representation of the chemical structure is shown for the sake of clarity. Selected interactions between residues are highlighted as dashed lines. Major interaction networks obtained from WISP analysis for C) α2β1 and D) α2β2 systems (close up views available in Figs. S9 and S10). (For interpretation of the references to colour in this figure legend, the reader is referred to the web version of this article.)

prone to adopt conformations suited to ATP binding. We speculate that this effect might be related, at least in part, to the occurrence of the β1Asn111 → β2Asp111 substitution, which would perturb the pattern of interactions formed by the activator upon binding to the ADaM site.

Disentangling the functional relevance of the perturbation caused by the β1Asn111 → β2Asp111 substitution is challenging in light of the presence of other substitutions present in β1 and β2 isoforms, which collectively may dictate the sensitivity of the AMPK complex to direct activators. In particular, changes of residues β1Phe82, β1Leu93 and β1Leu103 to β2Ile81, β2Ile92 and β2Ile103, respectively, which are embedded in a hydrophobic cluster in the CBM unit (Fig. S11), result not only in enlarged fluctuations of the hydrophobic core in holo α2β2, as the RMSF of these residues increases on average from 1.27 ± 0.05 (α2β1) to 1.57 ± 0.14 (α2β2) Å, but also to residue rearrangements, such as the conformational change observed for β2Tyr125 and β2Phe96, leading to local remodeling of the CBM unit (Fig. S12). At this point, it is worth noting that previous experimental studies reported that the double substitution β1Phe82 → Ile and β1Leu93 → Ile sufficed to annihilate the activation of α1β1γ1 by MT47-100 [31]. On the other hand, the linkage between βSer108p in the CBM unit and residues αLys29 and αLys31 in the P-loop is reinforced by secondary interactions formed by other residues, such as β1Thr106 and β1Arg107, which are changed to β2Ile106 and β2Lys107, respectively. β1Arg107 forms a cation-π interaction with βPhe112 (4.3 ± 0.9 Å), supplemented by a hydrogen bond with the carbonyl oxygen of βGly88. These interactions are lost in holo α2β2, where β2Lys107 is exposed to the aqueous solvent. Moreover, β1Thr106 is transiently hydrogen bonded to the carbonyl oxygen of αGly9, favouring the interaction of αArg10 with αGlu34, which is located at the end of the P-loop.

In the case of SC4, the resemblance of the dual interaction networks that connect the CBM unit and the P-loop via βSer108p and particularly the βArg83-SC4-αLys29 triad provides a basis to understand the mild selectivity between β1- and β2-containing AMPK. This can be attributed to the electrostatic influence of the carboxylate group present in SC4, which would facilitate the adoption of the two arrangements of βArg83 (βArg82), tempering the effect of the β1Asn111 → β2Asp111 substitution. Noteworthy, this may explain the slightly larger activation observed for β1-containing AMPK by 991, keeping in mind the similar scaffold of SC4 and 991, particularly regarding the presence of the carboxylate group (Table 1). On the other hand, these findings explain the moderate impact observed experimentally for the mutation βSer108 → Ala, which increase the EC_{50} value for SC4 activation by only ~ 4-fold (determined for α1β1γ1) [29], since this substitution can be counterbalanced by the βArg83-SC4-αLys29 network.

Further, this also explains the ~ 6-fold reduction in the activation potency (determined for α2β2γ1) found upon substitution of the SC4 pyridine-like nitrogen in the imidazo[4,5-b]pyridine ring for carbon [24], since this replacement should annihilate the hydrogen bond formed between SC4 and αLys29, altering the triad αLys29-imidazo[4,5-b]pyridine-αAsp88. At this point, let us note that this triad cannot be found in the X-ray structure of the complex between α2β2γ1 and SC4, since the crystallization experiment was performed at pH 6.0, where the imidazo[4,5-b]pyridine was protonated, leading to a different interaction pattern.

In summary, we were able to discern key molecular features that mediate the selective activation of α2β1 and α2β2 isoforms, explaining the different selectivity of A-769662 and SC4. These findings pave the way to understand the 'mechanically sensitive' role of specific residues in the ADaM site that are able to modulate the direct activation mechanism of β1- and β2-containing AMPK complexes. Further studies will be valuable to discern the structural basis of the different sensitivity of AMPK complexes formed by distinct α-subunits to the regulation by direct activators, thus enabling the design of tissue-selective modulators of this important energy sensor.

Funding

We thank the Spanish Ministerio de Economía y Competitividad (SAF2017-88107-R, and Maria de Maetzu MDM-2017-0767, AEI/FEDER), and the Generalitat de Catalunya (2017SGR1746) for financial support and the Barcelona Supercomputing Center (BCV-2014-3-0011 and BCV-2019-1-0009) and the Consorci de Serveis Universitaris de Catalunya (CSUC) for computational resources. E.A. thanks AGAUR (Generalitat of Catalunya; 2018FI-B1-00001) for a fellowship.

CRediT authorship contribution statement

Elnaz Aledavood: Formal analysis, Investigation, Visualization, Writing - original draft. **Alessia Forte:** Formal analysis, Investigation, Visualization, Writing - original draft. **Carolina Estarellas:** Conceptualization, Methodology, Investigation, Supervision, Writing - review & editing. **F. Javier Luque:** Conceptualization, Methodology, Investigation, Supervision, Writing - review & editing, Funding acquisition.

Declaration of Competing Interest

The authors declare that they have no known competing financial interests or personal relationships that could have appeared to influence the work reported in this paper.

Appendix A. Supplementary data

Supplementary data to this article can be found online at https://doi.org/10.1016/j.csbj.2021.05.056.

References

[1] Uhlen M, Oksvold P, Fagerberg L, Lundberg E, Jonasson K, Forsberg M, et al. Towards a knowledge-based human protein atlas. Nat Biotech 2010;28:1248–50.
[2] Uhlen M, Fagerberg L, Hallström BM, Lindskog C, Oksvold P, Mardinoglu A. Tissue-based map of the human proteome. Science 2015;347:1260419.
[3] Yang X, Coulombe-Huntington J, Kang S, Sheynkman GM, Hao T, Richardson A, et al. Widespread expansion of protein interaction capabilities by alternative splicing. Cell 2016;164:805–17.
[4] Eksi R, Li H-D, Menon R, Wen Y, Omenn GS, Ketzler M, et al. Systematically Differentiating Functions for Alternatively Spliced Isoforms Through Integrating RNA-seq Data. PLoS Comput Biol 2013;9:e1003314.
[5] Sulakhe D, S'Souza M, Wang S, Balasubramanian S, Athri P, Xie B, et al. Exploring the functional impact of alternative splicing of human protein isoforms using available annotation sources. Brief Bioinform 2019;20:1754–68.
[6] Menon R, Roy A, Mukherjee S, Belkin S, Zhang Y, Omenn GS. Functional implications of structural predictions for alternative splice proteins expressed in her2/neu-induced breast cancers. J Proteome Res 2011;10:5503–11.
[7] Chen H, Shaw D, Zeng J, Bu D, Jiang T. DIFFUSE: Predicting Isoform Functions From Sequences and Expression Profiles Via Deep Learning. Bioinformatics 2019;35:284–94.
[8] Thornton C, Snowden MA, Carling D. Identification of a Novel AMP-Activated Protein Kinase Beta Subunit Isoform That Is Highly Expressed in Skeletal Muscle. J Biol Chem 1998;273:12443–50.
[9] Cheung CF, Salt IP, Davies A, Hardie DG, Carling D. Characterization of AMP-activated protein kinase gamma subunit isoforms and their role in AMP binding. Biochem J 2000;346:659–69.
[10] Mahlapuu M, Johansson C, Lindgren K, Hjälm G, Barnes BR, Krook A, et al. Expression Profiling of the γ-Subunits Isoforms of AMP-Activated Protein Kinase Suggests a Major Role for γ 3 in White Skeletal Muscle. Am J Physiol Endocrinol Metab 2004;286:E194–200.
[11] Carling D, Mayer FV, Sanders MJ, Gamblin SJ. AMP-activated protein kinase: nature's energy sensor. Nat Chem Biol 2011;7:512–8.
[12] Herzig S, Shaw RJ. AMPK: guardian of metabolism and mitochondrial homeostasis. Nat Rev Mol Cell Biol 2018;19:121–35.
[13] Day EA, Ford RJ, Steinberg GR. AMPK as a therapeutic target for treating metabolic diseases. Trends Endocrinol Metab 2017;28:545–60.
[14] Luo Z, Saha AK, Xiang X, Ruderman NB. AMPK, the Metabolic Syndrome and Cancer. Trends Pharmacol Sci 2005;26:69–76.
[15] Hardie DG. AMP-activated protein kinase as a drug target. Annu Rev Pharmacol Toxicol 2007;47:185–210.
[16] Carling D. AMPK signalling in health and disease. Curr Opin Cell Biol 2017;45:31–7.
[17] Xiao B, Sanders MJ, Underwood E, Heath R, Carmena D, Jing C, et al. Structure of mammalian AMPK and its regulation by ADP. Nature 2011;472:230–3.
[18] Calabrese MF, Rajamohan F, Harris MS, Caspers NL, Magyar R, Withka JM, et al. Structural basis for AMPK activation: natural and synthetic ligands regulate kinase activity from opposite poles by different molecular mechanisms. Structure 2014;22:1161–72.
[19] Carling D, Thornton C, Woods A, Sanders MJ. AMP-activated protein kinase: new regulation, new roles?. Biochem J 2012;445:11–27.
[20] Chen L, Wang J, Zhang YY, Yan SF, Neumann D, Schlattner U, et al. AMP-activated protein kinase undergoes nucleotide-dependent conformational changes. Nat Struct Mol Biol 2012;19:716–8.
[21] Willows R, Sanders MJ, Xiao B, Patel BR, Martin SR, Read J, et al. Phosphorylation of AMPK by upstream kinases is required for activity in mammalian cells. Biochem J 2017;474:3059–73.
[22] Vazquez-Martin A, Vellon L, Quirós PM, Cufí S, De Galarreta ER, Ferraros CO, et al. Activation of AMP-activated protein kinase (AMPK) provides a metabolic barrier to reprogramming somatic cells into stem cells. Cell Cycle 2012;11:974–89.
[23] Cool B, Zinker B, Chiou W, Kifle L, Cao N, Perham M, et al. Identification and Characterization of a Small Molecule AMPK Activator That Treats Key Components of Type 2 Diabetes and the Metabolic Syndrome. Cell Metab 2006;3:403–16.
[24] Xiao B, Sanders MJ, Carmena D, Bright NJ, Haire LF, Underwood E, et al. Structural Basis of AMPK Regulation by Small Molecule Activators. Nat Commun 2013;4:1–10.
[25] Langendorf CG, Kemp BE. Choreography of AMPK activation. Cell Res 2015;25:5–6.
[26] Hardie DG. AMPK - Sensing Energy While Talking to Other Signaling Pathways. Cell Metab 2014;20:939–52.
[27] Olivier S, Foretz M, Viollet B. Promise and Challenges for Direct Small Molecule AMPK Activators. Biochem Pharmacol 2018;153:147–58.
[28] Willows R, Navaratnam N, Lima A, Read J, Carling D. Effect of different γ-subunit isoforms on the regulation of AMPK. Biochem J 2017;474:1741–54.
[29] Ngoei KRW, Langendorf CG, Ling NXY, Hoque A, Varghese S, Camerino MA, et al. Structural Determinants for Small-Molecule Activation of Skeletal Muscle AMPK α2β2γ1 by the Glucose Importagog SC4. Cell Chem Biol 2018;25:728–37.
[30] Cokorinos EC, Delmore J, Reyes AR, Albuquerque B, Kjøbsted R, Jørgensen NO, et al. Activation of Skeletal Muscle AMPK Promotes Glucose Disposal and Glucose Lowering in Non-Human Primates and Mice. Cell Metab 2017;25:1147–59.
[31] Scott JW, Galic S, Graham KL, Foitzik R, Ling NXY, Dite TA, et al. Inhibition of AMP-Activated Protein Kinase at the Allosteric Drug-Binding Site Promotes Islet Insulin Release. Chem Biol 2015;22:705–11.
[32] Aledavood E, Moraes G, Lameira J, Castro A, Luque FJ, Estarellas C. Understanding the Mechanism of Direct Activation of AMP-Kinase: Toward a Fine Allosteric Tuning of the Kinase Activity. J Chem Inf Model 2019;59:2859–70.
[33] Case DA, Ben-Shalom IY, Brozell SR, Cerutti DS, Cheatham TE, Cruzeiro VWD. AMBER 2018. San Francisco: University of California; 2018.
[34] Lindorff-Larsen K, Piana S, Palmo K, Maragakis P, Klepeis JL, Dror RO, et al. Improved Side-Chain Torsion Potentials for the Amber ff99SB Protein Force Field. Proteins 2010;78:1950–8.

[35] Wang J, Wolf RM, Caldwell JW, Kollman PA, Case DA. *Development and testing of a general AMBER force field. J Comput Chem* 2004;25:1157–74.
[36] Bayly CI, Cieplak P, Cornell W, Kollman PA. A well-behaved electrostatic potential based method using charge restraints for deriving atomic charges: the RESP model. J Phys Chem 1993;97:10269–80.
[37] Jorgensen WL, Chandrasekhar J, Madura JD, Impey RW, Klein ML. Comparison of simple potential functions for simulating liquid water. J Chem Phys 1983;79:926–35.
[38] Joung IS, Cheatham TE. Determination of alkali and halide monovalent ion parameters for use in explicitly solvated biomolecular simulations. J Phys Chem B 2008;112:9020–41.
[39] Amadei A, Linssen ABM, Berendsen HJC. Essential dynamics of proteins. Proteins 1993;17:412–25.
[40] Shkurti A, Goni R, Andrio P, Breitmoser E, Bethune I, Orozco M, et al. PyPcazip: A PCA-based toolkit for compression and analysis of molecular simulation data. SoftwareX 2015;5:44–50.
[41] Schlitter J. Estimation of Absolute And Relative Entropies Of Macromolecules Using The Covariance Matrix. Chem Phys Lett 1993;215:617–21.
[42] Baron R, Hünenberger PH, McCammon JA. Absolute single-molecule entropies from quasi-harmonic analysis of microsecond molecular dynamics: correction terms and convergence properties. J Chem Theory Comput 2009;5:3150–60.
[43] Harris SA, Gavathiotis E, Searle MS, Orozco M, Laughton CA. Cooperativity in drug-DNA recognition: a molecular dynamics study. J Am Chem Soc 2001;123:12658–63.
[44] Hunenberger P, Mark A, van Gunsteren W. Fluctuation and cross-correlation analysis of protein motions observed in nanosecond molecular dynamics simulations. J Mol Biol 1995;252:492–503.
[45] Bajusz D, Rácz A, Héberger K. Why is tanimoto index an appropriate choice for fingerprint-based similarity calculations?. J. Cheminform. 2015;7:20.
[46] O'Rourke KF, Gorman SD, Boehr DD. Biophysical and computational methods to aalyze amino acid interaction networks in proteins. Comput Struct Biotechnol J 2016;14:245–51.
[47] Van Wart AT, Durrant J, Votapka L, Amaro RE. Weighted implementation of suboptimal paths (WISP): an optimized algorithm and tool for dynamical network analysis. J Chem Theory Comput 2014;10:511–7.
[48] Dusan P, Lynn KSC. Molecular modeling of conformational dynamics and its role in enzyme evolution. Curr Opin Struct Biol 2018;52:50–7.
[49] Orellana L. Large-scale conformational changes and protein function: breaking the in silico barrier. Front. Mol. Biosci. 2019;6:117.
[50] Waheed SO, Ramanan R, Chaturvedi SS, Lehnert N, Schofield CJ, Christov CZ, et al. Role of Structural Dynamics in Selectivity and Mechanism of Non-Heme Fe(II) and 2-oxoglutarate-Dependent Oxygenases Involved in DNA Repair. ACS Cent Sci 2020;6:795–814.